Optica Applicata, Vol. XLVII, No. 3, 2017
DOI: 10.5277/oa170305

Improved method for passive ranging based on surface estimation of an airborne object using an infrared image sensor

DAVORIN L. MIKLUC, MILENKO S. ANDRIĆ, SRDJAN T. MITROVIĆ, BOBAN P. BONDŽULIĆ

Military Academy, University of Defence, Pavla Jurišića Šturma 33, 11000 Belgrade, Serbia

*Corresponding author: miklucd@yahoo.com

A new method for passive ranging using image size measurements from one sensor has been presented. The method relies on pixel filtration with histogram-based thresholding, followed by intensity and gradient magnitude analysis. Its efficiency and robustness were assessed in real infrared surveillance sequences, and it has proved to lead to better results than non-filtering techniques. The object distance estimation mean relative error does not exceed 3%, which implies that the suggested method enables precise range estimation based on object size measurements. To maximize the benefits of the suggested method, Kalman filter has been included in the algorithm in order to overcome fluctuations of the estimated object size.

Keywords: infrared sensor, passive ranging, pixel filtration, distance estimation.

1. Introduction

Passive sensors based object tracking systems can be used in various applications, such as video surveillance and security, speed control, air traffic control, missile guidance, weapon fire control, obstacle detection, robotics. Such systems can also be used to determine object distance, and the challenge is to get satisfactory performances when applying only one sensor [1–4]. There are many researches whose field of interest is tracking systems with one passive sensor, whether in daylight or at night [5–7]. In [8], a detail review of night vision technology is given. In cases of sensor saturation or major background fluctuations, approaches based on Beer–Lambert law and atmospheric propagation model do not generate reliable results [9].

One of the first researches which shows the solution on passive ranging based on image sequences is [10]. Research [11] is an enhancement of distance estimation based on intensity measurements when a sensor operates in saturation conditions. The accuracy of distance estimation in the approach which exploits scale changes depends on the method applied in image processing when determining the surface of the object. Passive

ranging is also treated in defence systems in a variety of atmospheric conditions [12]. Traditional intensity-based techniques for determining the segmentation threshold, such as [13, 14], are used for extraction and determination of its surface. A gradient-based object extraction method is reliable when the object intensity value differs significantly from the background intensity, which is not the case in infrared (IR) images [15]. The idea for searching, detecting and tracking an object smaller than 100 pixels has been presented in [16].

The idea proposed in this research is to join the intensity- and gradient-based methods and thus define a new approach to determining the contours. Pixel weighted coefficients in the analyzed gate are computed on the basis of intensity and gradient magnitude probability density functions. This idea is based on the new technique for motion detection that incorporates several innovative mechanisms, which were presented in [17], where the proposed technique stores a set of values taken in the past. Sequential importance sampling [18] is then used for pixel filtration (PF) based on normalized weighted coefficients. The suggested approach enables a more reliable estimation of the object surface, which directly decreases the error of object distance estimation. The error of the estimated distance to the object varies in time and directly depends on the quality of the object extraction. In the 1970s, Kalman developed an algorithm for optimal filtration for linear process with Gaussian noise measurement. Therefore, the suggested approach includes Kalman filter for filtration of the estimated object size fluctuations. The proposed method is recursive and improves distance estimation based on the surface of an airborne object in a frame in comparison to known methods for passive ranging with one sensor.

2. Method description

Figure 1 shows passive ranging process flow. A window gate, Fig. 1**b**, represents an adaptive rectangular window, whose dimensions are calculated based on the previously estimated object size. The window gate is isolated in each frame, within which pixel segmentation threshold I_T is defined using the algorithm suggested by OTSU [13]. The threshold value I_T is used in pixel filtration procedure. In infrared images, it is necessary to take the pixels whose intensity values are near the threshold because the contours of the object cannot be strictly defined. Gaussian distribution, which attributes a weight coefficient to every single pixel in the window gate, is suggested in [19]:

$$p_I^{(i)}(k) = \exp\left\{-\frac{1}{2}\left[\frac{I^{(i)}(k) - I_T(k)}{\sigma_I(k)}\right]^2\right\} \tag{1}$$

where $p_I^{(i)}(k)$ is the weight of i-th pixel based on pixel's intensity $I^{(i)}(k)$ at k-th frame, $I_T(k)$ is the intensity threshold in the current frame and $\sigma_I(k)$ is intensity variance for

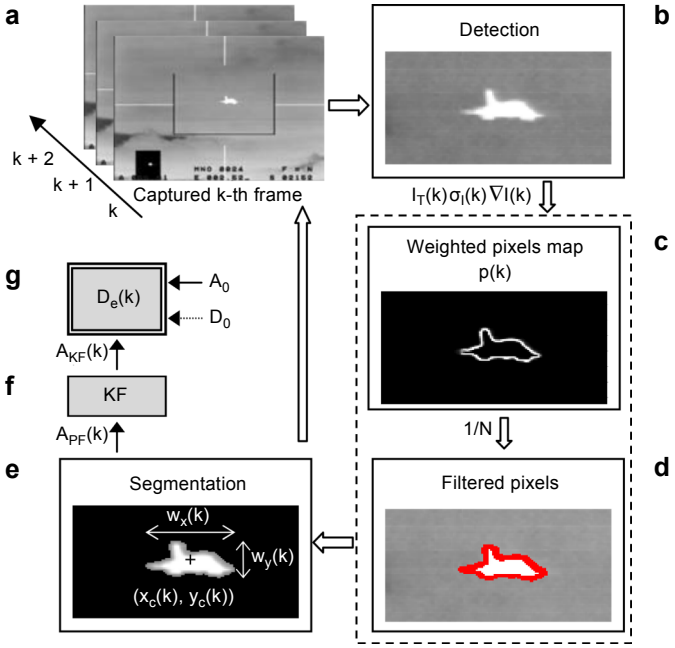

Fig. 1. Representation of the method flow (see text for explanation).

the window gate. The intensity variance is calculated using the following two equations:

$$I_{\mathrm{M}}(k) = \frac{1}{N}\sum_{i=1}^{N} I^{(i)}(k) \tag{2}$$

$$\sigma_{\mathrm{I}}^2(k) = \frac{1}{N-1}\sum_{i=1}^{N}\left[I^{(i)}(k) - I_{\mathrm{M}}(k)\right]^2 \tag{3}$$

where N is the number of pixels and I_{M} is mean pixel intensity in the window gate. It is assumed that the gradient magnitude is highest at the edges of the object, thus the Roberts operator is applied and the following distribution defined:

$$p_{\mathrm{G}}^{(i)}(k) = \exp\left[-\frac{1}{2}\left(\frac{\lambda}{\left\|\nabla I^{(i)}(k)\right\|}\right)^2\right] \tag{4}$$

where $\lambda = \max(\|\nabla I^{(1)}\|, \|\nabla I^{(2)}\|, \ldots, \|\nabla I^{(N)}\|)$ and $\nabla I^{(i)}$ is the i-th pixel gradient magnitude value. Weight coefficients from (1) and (4) need to be normalised, and then the joined weight coefficient for every pixel is defined as

$$p^{(i)}(k) = \frac{p_{\mathrm{I}}^{(i)}(k)}{\sum_{j=1}^{N} p_{\mathrm{I}}^{(j)}(k)} \frac{p_{\mathrm{G}}^{(i)}(k)}{\sum_{j=1}^{N} p_{\mathrm{G}}^{(j)}(k)} \tag{5}$$

Joined coefficients $p^{(i)}(k)$ are also normalised, with:

$$p_{\mathrm{J}}^{(i)}(k) = \frac{p^{(i)}(k)}{\sum_{j=1}^{N} p^{(j)}(k)} \tag{6}$$

Values of $p_{\mathrm{J}}^{(i)}(k)$ agree with pixel intensity in Fig. 1**c**, where brighter pixels represent larger values of $p_{\mathrm{J}}^{(i)}(k)$.

Pixel filtration is performed on the basis of weight coefficients and filtering threshold value of $1/N$. The idea for such filtering has been derived from a sequential importance sampling method, commonly used in particle filters framework [18]. Filtered pixels represent the area of the object contours $A_{\mathrm{PF}}(k)$, and they are highlighted in Fig. 1**d**.

The sum of filtered pixels and pixels within the enclosed contour of the filtered pixels, Fig. 1**e**, represents the estimated size of the object $A_{\mathrm{PF}}(k)$. In the ideal video sequence, the object size increases while the object is approaching, and decreases while it is moving away from the sensor, *i.e.*, its change in size is monotonously following the distance change. The presence of noise and the fact that the edges of the object are not clear in infrared images are the main factors influencing the fluctuation of $A_{\mathrm{PF}}(k)$ estimations in real applications. The usage of Kalman filter (KF) – see Fig. 1**f** – with the filtration model of constant acceleration for object size estimation $A_{\mathrm{KF}}(k)$ has been suggested for overcoming fluctuations of $A_{\mathrm{PF}}(k)$. This model has been accepted, knowing that the size change follows the quadratic law. The state vector is accepted as

$$X(k) = \left[A(k) \quad \dot{A}(k) \quad \ddot{A}(k)\right]^T \tag{7}$$

where states of $X(k)$ are: area of object $A(k)$, rate of area change $\dot{A}(k)$ and acceleration of area change $\ddot{A}(k)$. The Kalman filter relations are [20]:

$$\hat{X}(k) = FX(k) \tag{8}$$

$$\hat{P}(k) = FP(k-1)F^T + GQG^T \tag{9}$$

$$W(k) = \hat{P}(k)H^T\left[H\hat{P}(k)H^T + R\right]^{-1} \tag{10}$$

$$X(k) = \hat{X}(k) + W(k)\left[A_{\mathrm{PF}}(k) - H\hat{X}(k)\right] \tag{11}$$

$$A_{\mathrm{KF}}(k) = HX(k) \tag{12}$$

$$P(k+1) = \left[I - W(k)H\right]\hat{P}(k) \tag{13}$$

$$G = \begin{bmatrix} T^2/2 & T & 1 \end{bmatrix} \tag{14}$$

$$Q = 1 \text{ pixel}^2/\text{s}^4 \tag{15}$$

$$R = [1 \quad 0 \quad 0] \text{ pixel}^2 \tag{16}$$

$$F = \begin{bmatrix} 1 & T & T^2/2 \\ 0 & 1 & T \\ 0 & 0 & 1 \end{bmatrix} \tag{17}$$

$$H = [1 \quad 0 \quad 0] \tag{18}$$

where pixel represents a measurement unit for the object surface and T is a sampling interval.

The estimated distance D_e (see Fig. 1**g**) is calculated based on the filtered object area A_{KF}, initial object area A_0 and initial distance to the object D_0.

3. Pseudo-synthetic sequence

Pseudo-synthetic sequence is formed of an airborne object from one video sequence and the background from the other video sequence, Fig. 2. It lasts for 350 frames with the frame rate of 30 fps. The airborne object area in a frame is a constant value of $A_T(k) = 259$ pixels, Fig. 3. This simulation works under an assumption that an airborne object does not change an attitude or make a maneuver and during the simulation, dis-

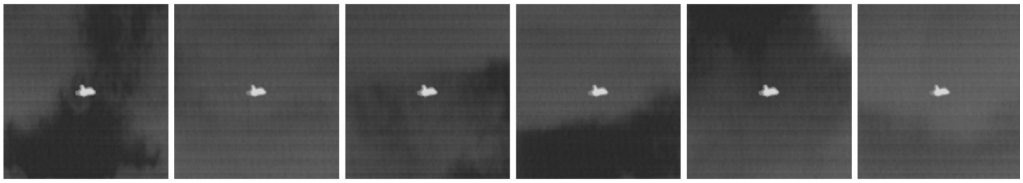

Fig. 2. Example frames from pseudo-synthetic sequence.

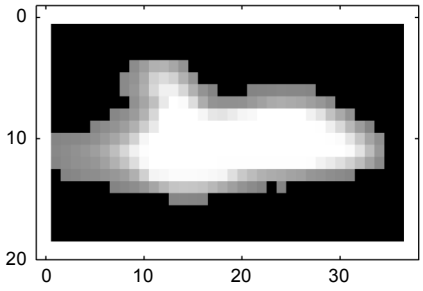

Fig. 3. The formed airborne object area.

tance is constant. Minimal intensity value of the airborne object is $I_{\min} = 110$. Two scenarios have been analyzed, where the main task is to estimate the airborne object area and then evaluate the proposed method. The minimum intensity of the airborne object is higher than the intensity of the background and in the second one, the intensity of airborne object is decreased for 20, which implies the edge detection problem. The criterion of a relative area error is adopted as an evaluation method,

$$E_{\mathrm{rrA}}(k) = \frac{\left|A_{\mathrm{e}}(k) - A_{\mathrm{T}}(k)\right|}{A_{\mathrm{T}}(k)} \times 100\% \tag{19}$$

The following figures represent the parameter estimation, which are compared with results using standard segmentation methods of Otsu and Tsai.

The estimated airborne object area $A_{\mathrm{e}}(k)$ is represented in Figs. 4**a** and 5**a**, while the relative area error, $E_{\mathrm{rrA}}(k)$, is shown in Figs. 4**b** and 5**b**. The other estimated parameters can be seen in Figs. 4**c**, 4**d**, 5**c** and 5**d**. Considering the values of $A_{\mathrm{e}}(k)$ and $E_{\mathrm{rrA}}(k)$, the proposed method has a better area estimation than standard methods.

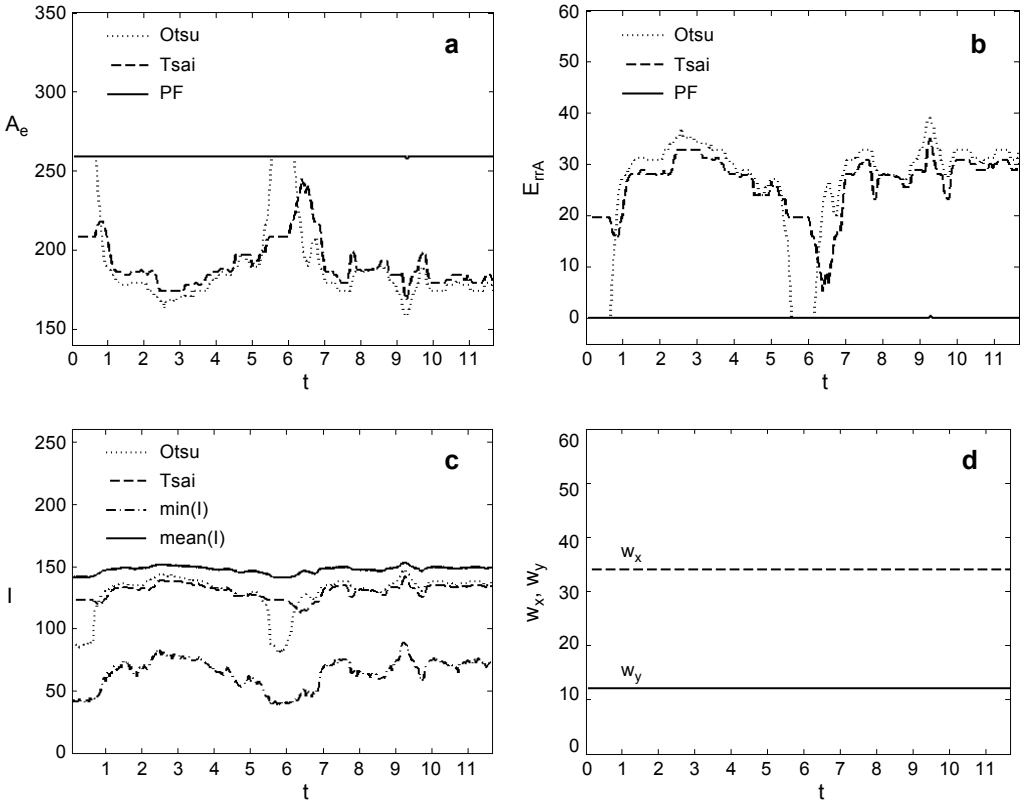

Fig. 4. Estimated parameters: the airborne object area (**a**), the relative area error (**b**), intensity in the window gate (**c**), and the airborne object dimensions (**d**); $I_{\min} = 110$.

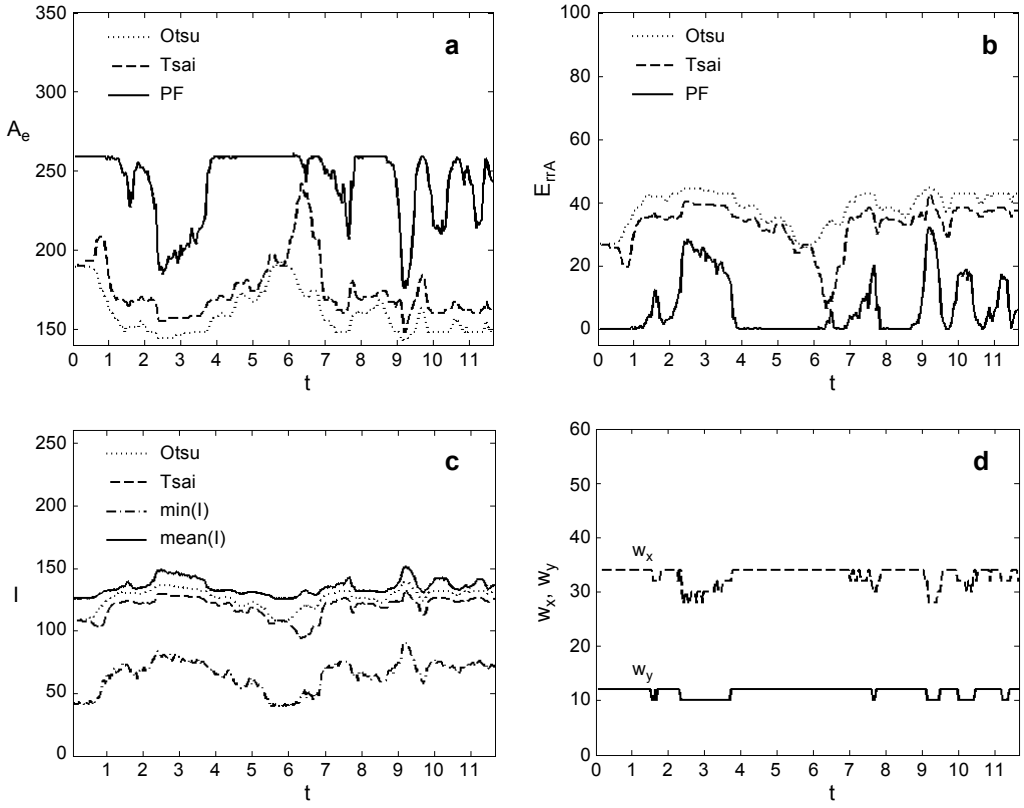

Fig. 5. Estimated parameters: the airborne object area (**a**), the relative area error (**b**), intensity in the window gate (**c**), and the airborne object dimensions (**d**); $I_{\min} = 90$.

The described method gives good results whether the airborne object intensity is higher than the background intensity or absorbed in it. The results in Figs. 4**c** and 5**c** represent the intensity threshold, which is very important for a recursive algorithm. The expected position of the airborne object in frame depends on its center and size estimation. Figure 4**d** shows perfect airborne object size estimation when its intensity is over 110, while Fig. 5**d** represents very slight fluctuation when the airborne object intensity is within background intensity. To sum up, these results justify the proposed recursive method, which can be easily used for distance estimation based on size measurements.

4. Experiments

The proposed method was tested in three real infrared image sequences recorded by dual observer passive ranging system (DOPRS) [9], which is designated for tracking airborne objects. The system uses two thermal cameras to estimate the object distance

by triangulation, with the absolute error less than five metres. Sequences recorded by one camera were used in this research, while distance obtained by DOPRS was used in analyzes as the reference in determining the estimation error. Based on the object size, distance $D_e(k)$ is estimated by [21]

$$D_e(k) = D_0 \sqrt{\frac{A_0}{A_e(k)}}, \quad e \in \{KF, PF, Ot, Ts\} \tag{20}$$

where A_e denotes the estimated object area as: A_{KF} – estimated according to algorithm in Fig. 1, A_{PF} – calculated by the same algorithm without Kalman filter (see Fig. 1**f**), areas A_{Ot} and A_{Ts} are the outputs of block sequence **a** → **b** → **e** → **g** in Fig. 1 and the corresponding method for intensity threshold calculation: Otsu's [13] and Tsai's methods [14], respectively.

Estimated object width $w_x(k)$ and height $w_y(k)$ are used for adaptation and calculation of the new window gate size, which is three times larger than the object. The new window gate is positioned at the estimated center of the object $(x_c(k), y_c(k))$ which is calculated by simple mean of the position of object pixels by coordinates x and y. As a new window gate is being generated for object detection, an optimal intensity threshold is provided.

The airborne object is moving towards the sensor in all the sequences that last for N_T frames. The background is on a nearly constant grey level in the first sequence, Fig. 6**a**, while the background intensity fluctuates in the second sequence, Fig. 6**b**.

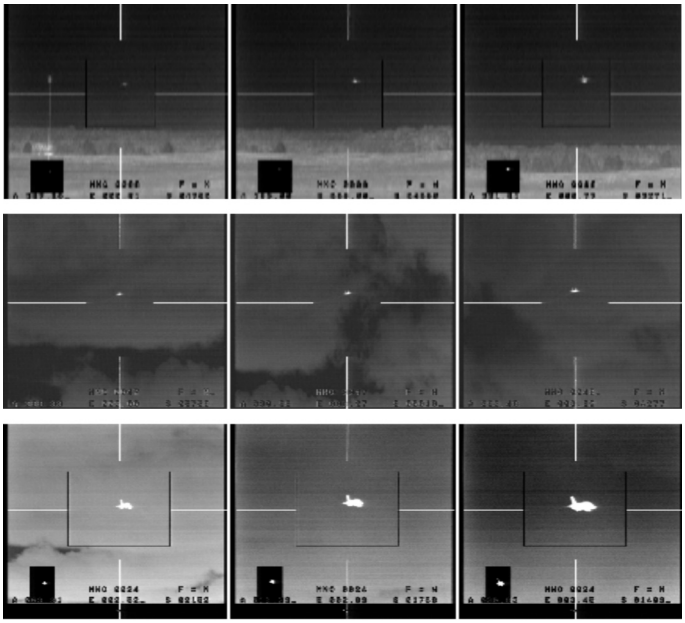

Fig. 6. Example frames from real sequences: first (**a**), second (**b**), and third (**c**).

The object intensity is saturated in the third sequence, Fig. 6**c**. Selected video sequences were previously analyzed in [9], where Tsai's method [14] was used to calculate the intensity threshold.

Object distances were determined by Eq. (20), where D_0 was taken over from DOPRS. Object surfaces were estimated by the proposed method, Fig. 1, and two histogram -based techniques: Tsai's moment-based thresholding [14] and Otsu's method [13], without weighting and filtration blocks in Fig. 1. The results are presented in distance estimation graphs (Figs. 7–9) and mean relative error of the distance value for every sequence (see the Table) using the following equation:

$$\overline{E}_{\mathrm{rrD}} = \frac{\sum_{k=1}^{N_\mathrm{T}} E_{\mathrm{rrD}}(k)}{N_\mathrm{T}} \tag{21}$$

Object distance estimation in the first video sequence is shown in Fig. 7, where D stands for DOPRS distance, D_{Ts} is the distance estimated by Tsai based approach,

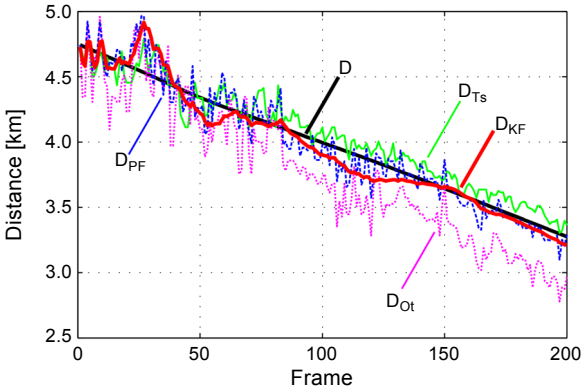

Fig. 7. Distance estimation for the first sequence.

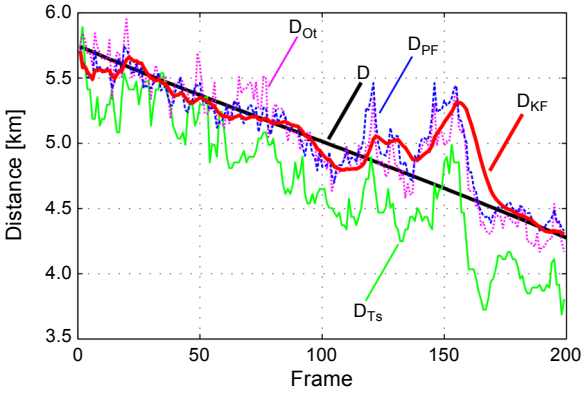

Fig. 8. Distance estimation for the second sequence.

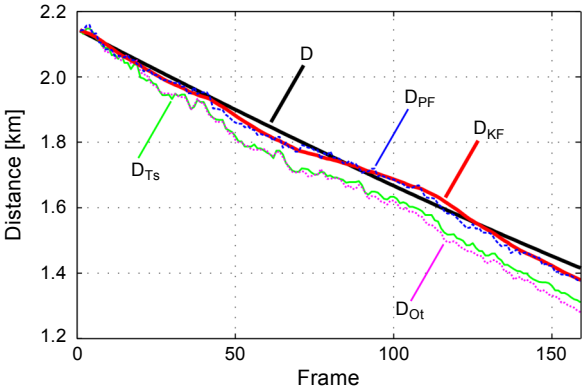

Fig. 9. Distance estimation for the third sequence.

T a b l e. Mean relative error of distance.

	Sequence		
Method	First	Second	Third
Tsai	2.38%	6.77%	3.64%
Otsu	6.85%	2.79%	4.29%
Pixel filtration	2.28%	2.89%	1.16%
Pixel filtration (KF included)	**1.67%**	**2.71%**	**1.10%**

D_{Ot} represents estimation relying on Otsu's method and D_{PF} is the distance obtained using the method suggested in this research. The blurred object edges in the IR sequence cause the variations in object size measurements and distance estimation using pixels filtration and traditional methods, which justifies the application of Kalman filter. It can be seen that D_{PF} is of a slightly smaller distance estimation variance in comparison to D_{Ts}, while the result is significantly better than D_{Ot}, since the estimated distance D_{KF} is of the smallest variations, as expected.

Figure 8 shows that the suggested method has the smaller distance estimation error, except in cases of drastically changed background intensity, and then the distance estimation by Otsu's method proves slightly better. As in the previous sequence, the estimated distance on Kalman filter output shows the lowest error.

Justifiability of the method presented in this research is best seen in Fig. 9, where distance estimation is nearly ideal. Other two methods give less reliable distance estimations when the object intensity is saturated. In this sequence, the object surface is relatively large (Fig. 6**c**), and the contribution of Kalman filter is not obvious as in the preceding sequences.

According to the results in the Table, it is evident that the proposed method is robust as it estimates object distance with errors below 3% in all the analyzed sequences, while the distance estimation error by non-filtration techniques notably depends on the sequence.

5. Conclusion

The robust method for distance estimation using a single sensor, involving Otsu's method for intensity threshold and pixel filtration using intensity and gradient magnitude, has been proposed. It was shown that mean relative error is under 3% in all the analyzed scenarios, and below 2% for approximately constant backgrounds. The suggested pixel filtration method for object size measurement with Kalman filter produces significantly better results for distance estimation in comparison to traditional methods. The important contribution is visible in the sequences with distanced objects of small surfaces on nearly constant backgrounds, while the most significant results are obtained from the sequence with saturated object intensity. Further research will be focused on minimising a distance estimation error under complicated backgrounds.

Acknowledgements – This work has been partially supported by the Ministry of Education, Science and Technological Development of the Republic of Serbia under Grant III-47029.

References

[1] Anderson J.R., Hawks M.R., Gross K.C., Perram G.P., *Flight test of an imaging O_2(X-b) monocular passive ranging instrument*, Proceedings of SPIE **8020**, 2011, article ID 802005.

[2] Diao W.-H., Mao X., Chang L., Jiang L., *Operating distance evaluation method for infrared imaging system under complicated backgrounds*, Electronics Letters **45**(25), 2009, pp. 1309–1310.

[3] Benet G., Blanes F., Simó J.E., Pérez P., *Using infrared sensors for distance measurement in mobile robots*, Robotics and Autonomous Systems **40**(4), 2002, pp. 255–266.

[4] Jian-Zhong Xu, Zu-Lin Wang, Yi-Huan Zhao, Xu-Jing Guo, *A distance estimation algorithm based on infrared imaging guided*, International Conference on Machine Learning and Cybernetics, Vol. 4, 2009, pp. 2343–2346.

[5] Zappi P., Farella E., Benini L., *Tracking motion direction and distance with pyroelectric IR sensors*, IEEE Sensors Journal **10**(9), 2010, pp. 1486–1494.

[6] Srivastava H.B., Limbu Y.B., Saran R., Kumar A., *Airborne infrared search and track systems*, Defence Science Journal **57**(5), 2007, pp. 739–753.

[7] De Visser M., Schwering P.B.W., De Groot J.F., Hendriks E.A., *Passive ranging using an infrared search and track sensor*, Optical Engineering **45**(2), 2006, article ID 026402.

[8] Chrzanowski K., *Review of night vision technology*, Opto-Electronics Review **21**(2), 2013, pp. 153 –181.

[9] Bondžulić B.P., Mitrović S.T., Barbarić Ž.P., Andrić M.S., *A comparative analysis of three monocular passive ranging methods on real infrared sequences*, Journal of Electrical Engineering **64**(5), 2013, pp. 305–310.

[10] Atherton T.J., Kerbyson D.J., Nudd G.R., *Passive estimation of range to objects from image sequences*, Proceedings of the British Machine Vision Conference, Springer, London, 1991, pp. 343–346.

[11] Mitrović S.T., Bondžulić B.P., Andrić M.S., Barbarić Ž.P., *The statistical approach for overcoming the sensor saturation effect in passive ranging*, Elektronika ir Elektrotechnika **20**(2), 2014, pp. 52–57.

[12] Hoonkyung Cho, Joohwan Chun, Doochun Seo, Seokweon Choi, *Range estimation of passive infrared targets through the atmosphere*, Optical Engineering **52**(4), 2013, article ID 046402.

[13] Otsu N., *A threshold selection method from gray-level histograms*, IEEE Transactions on Systems, Man, and Cybernetics **9**(1), 1979, pp. 62–66.

[14] WEN-HSIANG TSAI, *Moment-preserving thresholding: a new approach*, Computer Vision, Graphics, and Image Processing **29**(3), 1985, pp. 377–393.
[15] YILMAZ A., SHAFIQUE K., SHAH M., *Target tracking in airborne forward looking infrared imagery*, Image and Vision Computing **21**(7), 2003, pp. 623–635.
[16] SUNGHO KIM, JOOHYOUNG LEE, *Small infrared target detection by region-adaptive clutter rejection for sea-based infrared search and track*, Sensors **14**(7), 2014, pp. 13210–13242.
[17] BARNICH O., VAN DROOGENBROECK M., *ViBe: a universal background subtraction algorithm for video sequences*, IEEE Transactions on Image Processing **20**(6), 2011, pp. 1709–1724.
[18] JUN S. LIU, RONG CHEN, LOGVINENKO T., *A theoretical framework for sequential importance sampling with resampling*, [In] *Sequential Monte Carlo Methods in Practice*, Springer, 2001, pp. 225–246.
[19] CHENGEN LU, LATECKI L.J., GUANGXI ZHU, *Contour extraction using particle filters*, [In] *Advances in Visual Computing*, Lecture Notes in Computer Science, Vol. 5359, Springer, 2008, pp. 192–201.
[20] BLACKMAN, S.S., *Multiple-Target Tracking with Radar Applications*, Artech House, 1986, pp. 26–27.
[21] BARBARIC Z.P., BONDZULIC B.P., MITROVIC S.T., *Passive ranging using image intensity and contrast measurements*, Electronics Letters **48**(18), 2012, pp. 1122–1123.

Received September 20, 2016
in revised form December 8, 2016